JOURNAL OF COMPUTATIONAL PHYSICS 40, 36–63 (1981)

Some Response Characteristics of Finite-Element Tidal Models

GEORGE W. PLATZMAN

Department of the Geophysical Sciences, The University of Chicago, Chicago, Illinois 60637

Received March 6, 1980

Small-scale error can arise in finite-element tidal models from different aspects of the spatial discretization. One source is incompatibility in smoothness of interpolation of the pressure and velocity fields. Noise of this type can be eliminated completely by using Stokes/Helmholtz potentials to represent the velocity, and interpolating these potentials with the same smoothness as is given to the pressure. Another source is inhomogeneous triangulation, in which the number of links is not the same at all nodes. Noise of this type can be suppressed by using a high-resolution grid (the resolution in question being that of the response rather than of the domain). These points are illustrated by examining the response characteristics of idealized models. It is found that in the models considered, small-scale noise can be ascribed to resonance anomalies associated with the method of spatial discretization. In this analysis the time is continuous, but some remarks are appended on the effect of time discretization, and a formal proof is given of the time-stepping stability of a general, discretized form of Laplace's tidal equations.

1. INTRODUCTION

The use of finite elements for modelling oceanic tidal phenomena is providing a growing base of experience in the design of such models. The merits of various procedures were examined recently by Gray and Lynch (1977, 1978) and Lynch and Gray (1979). The present note is prompted by their work and extends some remarks of my own (Platzman, 1978, Appendix A; see also Luskin, 1979).

Lynch and Gray observe that a common defect of finite-element tidal models is the generation of small-scale error, typically with a wave length near the smallest resolvable by the grid (sometimes called "$2\delta x$ noise"). I intend here to examine two sources of such noise, one arising from the method of discretizing the velocity field, the other from the grid triangulation. The former occurs in both one- and two-dimensional models and can be eliminated in a simple way. The latter is inherently two dimensional and can be diminished by increasing the spatial resolution of the response or by changing the triangulation. The two models used below to illustrate these suggestions are not realistic tidal models in the strict sense because they do not include frictional or Coriolis forces and are limited to longitudinal oscillations on a shelf of uniform depth. Nevertheless, they suffice for the purpose intended, namely, to

0021-9991/81/030036-28$02.00/0

examine some response characteristics implicit in standard finite-element methods of discretizing Laplace's tidal equations.

The usual procedure for solving finite-element equations is by direct numerical calculation through matrix inversion. It is well known, however, that grid triangulations with a high degree of symmetry can lead in some cases to finite-element equations that are equivalent to simple finite-difference equations. This study is limited to such cases, and moreover, the models will be simplified to an extent that permits straightforward analytic solutions to be found for the difference equations encountered. It is from such solutions that the response of the model is calculated. This procedure has the merit of providing a clear view of the mathematial structure of the response.

To simplify the task of finding analytic solutions I discretize the continuum equations only in the spatial independent variables. The justification for retaining the time as a continuum variable is not merely prudential: by doing so we can isolate the effects of spatial discretization and thus more readily compare the responses of different models. However, if the time is idscretized, it is a simple matter to modify the solutions in the particular cases considered, and I indicate at the end how this can be done.

2. Free Oscillations in a One-Dimensional Model

For preliminary illustration consider one-dimensional longitudinal free oscillations in a closed channel of length L and depth h, governed by the linearized, hydrostatic equations

$$\partial\zeta/\partial t = -\partial u/\partial x; \tag{2.1a}$$

$$\partial u/\partial t = -gh\,\partial\zeta/\partial x. \tag{2.1b}$$

Here ζ is elevation of the free surface above mean level and u the x-component of volume transport (depth times velocity). Weighted-residual forms of (2.1) are

$$\int_0^L \alpha^i(\partial\zeta/\partial t)\,dx = \int_0^L (\partial\alpha^i/\partial x)\,u\,dx, \tag{2.2a}$$

$$\int_0^L \beta^j(h^{-1}\,\partial u/\partial t)\,dx = \int_0^L \beta^j(-g\,\partial\zeta/\partial x)\,dx, \tag{2.2b}$$

where α^i and β^j are sets of weight functions for the mass and momentum equations, respectively. The right-hand side of (2.2a) implies partial integration of the right-hand side of (2.1a) and omission of the boundary term $\alpha^i u$ because in this first model we want $u = 0$ at both ends of the channel.

In finite-element methods the weight functions are localized. I assume, further, that each α^i is continuous and is the discrete analogue of a delta function, and accordingly

that in the limit of zero discretization (2.2a) converges to (2.1a). For the β^j of (2.2b) I consider two general alternatives: (i) the β^j are like the α^i and in the limit of zero discretization cause (2.2b) to converge to (2.1b); or (ii) each β^j is the x-derivative of a discrete delta function and in the limit of zero discretization causes (2.2b) to converge to the x-derivative of (2.1b). (In the latter case the β^j are not necessarily continuous.) To have a convenient terminology I will refer to finite-element models of these two types as "primitive" and "derivative" models, respectively.

A rudimentary example of a primitive model is the standard finite-element procedure (for example, see Connor and Brebbia, 1976, Chap. 7) in which ζ and u are discretized on the same grid of nodes and are represented by the same set of basis functions. In this procedure, moreover, the basis functions are adopted as weight functions (Galerkin's method). Thus, let $x = i\delta x$ $(i = 0, 1, 2, \ldots, n)$ be the locations of equally-spaced nodes and take $\beta^i = \alpha^i$ to be piecewise-linear bases and weights. Then for uniform depth the difference equations that arise from (2.2) at internal points are

$$(\partial/\partial t)(1 + 2\mu^2)\,\zeta/3 = -\mu\delta u/\delta x, \tag{2.3a}$$

$$(\partial/\partial t)(1 + 2\mu^2)\,u/3 = -c^2\mu\delta\zeta/\delta x, \tag{2.3b}$$

where μ and δ are central smoothing and first-difference operators

$$\begin{aligned} \mu f(x) &\equiv \tfrac{1}{2}[f(x + \tfrac{1}{2}\delta x) + f(x - \tfrac{1}{2}\delta x)], \\ \delta f(x) &\equiv f(x + \tfrac{1}{2}\delta x) - f(x - \tfrac{1}{2}\delta x), \end{aligned} \tag{2.4}$$

and $c \equiv (gh)^{1/2}$ is the speed of propagation of long gravity waves.

At the end points, where the channel is closed, rigid-boundary coastal conditions

$$u_0 = 0; \tag{2.5a}$$

$$u_n = 0 \tag{2.5b}$$

are imposed as essential boundary conditions and take the place of (2.2b). However, ζ is not constrained at the end points so (2.2a) must be applied there. It is convenient to state the result in the same form (2.3a) as used for internal points, and this can be done provided we make use of external nodes $i = -1$ and $i = n + 1$ such that

$$\zeta_{-1} = \zeta_1; \qquad u_{-1} = -u_1, \tag{2.6a}$$

$$\zeta_{n+1} = \zeta_{n-1}; \qquad u_{n+1} = -u_{n-1}. \tag{2.6b}$$

These reflection conditions are appropriate only for a rigid boundary.

Equations (2.3)–(2.6) are linear difference equations with constant coefficients. They have the oscillatory solutions

$$\begin{aligned} \zeta &= A \cos kx \cos \sigma t, \\ u/c &= A \sin kx \sin \sigma t, \end{aligned} \tag{2.7a}$$

$$\sigma d/c = (3 \sin kd)/(2 + \cos kd), \tag{2.7b}$$

where $d \equiv \delta x$ and k is a wave number for which $\sin kL = 0$:

$$k = (1, 2, 3, \ldots, n-1)\,\pi/L. \tag{2.8}$$

In addition there are two steady solutions, which can be obtained from (2.7) by setting $k = 0$ and $k = n\pi/L = \pi/d$. In both of these $u = 0$ identically, while $\zeta = A$ (uniform surface elevation) in the former and $\zeta = (-1)^j A$ (stationary wave of length $2d$) in the latter. It should be understood that (2.7a) gives the values of ζ, u only at the nodes $x = (0, 1, 2, \ldots, n)\,d$ of the grid. Between the nodes the finite-element model calls for ζ, u to be interpolated linearly rather than trigonometrically. It is apparent that (2.7) converges to the normal modes of the continuum equations (2.1) in the limit $d \to 0$, since (2.7b) makes $\sigma \to kc$ in that limit.

In Fig. 1 curve P (signifying a primitive model) is a graph of the frequency equation (2.7b). If $kd \ll 1$ (a well-resolved mode), the right-hand side of (2.7b) $= kd + O(kd)^5$ so $\sigma = kc[1 + O(kd)^4]$. Thus (2.7b) gives a very good account of the well-resolved modes. However, the remarkable feature of curve P is that it reaches a maximum frequency ($3^{1/2}$ on the ordinate scale) and then declines to zero at the maximum wave number $k = \pi/d$. The "folding" wave number is $2\pi/3d$. Its presence causes the frequency of every mode with wave length less than $3d$ to be aliased into the low frequencies that belong to waves of large scale. In other words, in the one-dimensional finite-element primitive model, all frequencies are aliased that belong to the upper one-third of the resonant wave numbers.

A consequence of the aliasing must be that when a finite-element model of this type is used to generate a forced motion (for example, by including a tidal force on the right-hand side of the momentum equation), the response will have a noise component with wave length between $2d$ and $3d$, as well as the larger wave length physically appropriate to the forcing frequency. The cause of this peculiar error is that in their finite-element representations ζ and u were given the same degree of "smoothness." In the above example, piecewise-linear approximation was used for both variables. The aliasing that this creates is illustrated strikingly by the steady solutions previously mentioned, both with $u = 0$ at all nodes. The one with ζ uniform

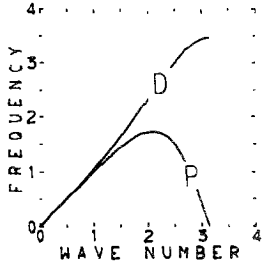

FIG. 1. Resonance frequency $\sigma d/c$ as a function of wave number kd for free oscillations of one-dimensional models. Curve P (primitive model) is a graph of Eq. (2.7b), curve D (derivative model) of (2.13b). In the former case u is interpolated linearly between nodes; in the latter u is uniform between modes. In both cases ζ is interpolated linearly.

and $k = 0$ is the solution physically appropriate to zero frequency (and is equal to the continuum steady solution). The one with the "sawtooth" structure $\zeta \sim (-1)^i$ and $k = \pi/d$ is the alias. It clearly has no physical counterpart. Its existence as a solution of (2.3) is a result of choosing both α and β in (2.2) as piecewise-linear bases. That choice causes the integral representing the pressure-gradient force (the right-hand side of (2.2b)) to take an average of the gradient of ζ in two adjoining elements, as is evident from the presence of the operator $\mu\delta$ in (2.3b). This average is clearly zero for the sawtooth wave. In other words, the finite-element model is unable to detect the pressure gradient in the sawtooth wave and consequently permits this deformation of the free surface to persist without particle displacements, in violation of the laws of dynamics.

A remedy for aliasing of this type is to give the same degree of smoothness to u and the *gradient* of ζ. Since ζ must be continuous (as it is a proxy for pressure), it must be interpolated at least linearly. If that choice is made, then u must be uniform within elements (and therefore discontinuous between them) in order to have the same degree of smoothness as $\partial\zeta/\partial x$. An expedient way to represent the transport in this manner is by means of Stokes/Helmholtz potentials. In one dimension $u = -h\,\partial\phi/\partial x$, and the potential ϕ is discretized at the ζ-nodes using the ζ-bases α^i. The corresponding finite-element equations are (Platzman, 1978, Eqs. (4.9a), (4.9b))

$$\int_0^L \alpha^i \frac{\partial\zeta}{\partial t}\,dx = \int_0^L \frac{\partial\alpha^i}{\partial x}\left(-h\frac{\partial\phi}{\partial x}\right)dx, \tag{2.9a}$$

$$\int_0^L \frac{\partial\alpha^i}{\partial x}\frac{\partial}{\partial t}\left(-h\frac{\partial\phi}{\partial x}\right)dx = \int_0^L \frac{\partial\alpha^i}{\partial x}\left(-gh\frac{\partial\zeta}{\partial x}\right)dx. \tag{2.9b}$$

These are equivalent to (2.2) if in the momentum equation (2.2b) the weight function β^j is taken as $h\,\partial\alpha^i/\partial x$. The effect of this choice is to cause (2.9b) to converge, in the limit of zero discretization, to the derivative $\partial/\partial x$ of (h times) the momentum equation. Thus we have an example of what I referred to previously as a "derivative" model. The boundary condition $u = 0$, imposed as an essential condition in the primitive model, is a natural condition for (2.9). (In two dimensions two scalar potentials are used and the derivative model of the vector momentum equation consists of two scalar equations one of which converges to the divergence of h times the momentum equation, the other to the vorticity of the momentum equation.)

To solve (2.9) note that (2.9b) requires $\partial\phi/\partial t - g\zeta$ to be uniform in x. In particular we can take $\partial\phi/\partial t = g\zeta$, since an arbitrary function of t alone can be added to ϕ without altering (2.9). This makes it possible to eliminate ϕ by applying $\partial/\partial t$ to (2.9a), thereby producing the finite-element wave equation

$$\int_0^L \alpha^i \frac{\partial^2\zeta}{\partial t^2}\,dx = -\int_0^L \frac{\partial\alpha^i}{\partial x}\,gh\frac{\partial\zeta}{\partial x}\,dx. \tag{2.10}$$

When α^i is piecewise linear and h is uniform, (2.10) leads at internal nodes to the difference equation

$$(\partial^2/\partial t^2)(1 + 2\mu^2)\,\zeta/3 = c^2\delta^2\zeta/(\delta x)^2. \tag{2.11}$$

At the end points the difference equations that arise from (2.10) are correctly rendered by (2.11) supplemented with rigid-boundary reflection conditions

$$\zeta_{-1} = \zeta_1; \tag{2.12a}$$

$$\zeta_{n+1} = \zeta_{n-1}. \tag{2.12b}$$

The solution of (2.11)–(2.12) for free oscillations is

$$\zeta = A \cos kx \cos \sigma t, \tag{2.13a}$$

$$\phi\sigma/g = A \cos kx \sin \sigma t, \tag{2.13b}$$

$$\sigma d/c = [6(1 - \cos kd)/(2 + \cos kd)]^{1/2},$$

provided k is a wave number that makes $\sin kL = 0$:

$$k = (1, 2, 3, \ldots, n)\,\pi/L.$$

In addition there is a steady solution ($\sigma = 0$) that can be derived from (2.13) by setting $k = 0$, namely, $\zeta = A$ (uniform elevation), $\phi = gAt$ (zero velocity).

In Fig. 1 curve D (derivative model) shows the *monotonic* spectrum produced by the frequency function (2.13b). For well-resolved modes ($kd \ll 1$) we now have $\sigma = kc[1 + O(kd)^2]$. Although the error is larger than that of model P, where it is of order $(kd)^4$, the derivative model is free of aliasing. Incidentally, it should not be inferred that aliasing is inherent in primitive models, as can be seen for example by using linear interpolation for u and quadratic for ζ. Likewise, derivative models are not inherently free of aliasing, as becomes evident by using quadratic interpolation for ϕ and linear for ζ.

At first sight aliasing may seem to be a fatal defect. Indeed, in the context of an eigenvalue calculation (Platzman, 1978) it causes serious, perhaps insurmountable difficulties. However, in a tidal calculation a smooth response is possible in spite of aliasing, because the resonance cross section of an aliased mode is very small when the grid interval is small enough to give good resolution to the principal wave length of the response. The example next to be discussed is designed to illustrate this point.

3. Application to One-Dimensional Tidal Models

The simplest adaptation of the foregoing analysis to tidal models is for the problem of tides on a continental shelf. Let $x = 0$ be the location of the coast and $x = L$ the shelf break, where the water on the self is in direct contact with that of the deep

ocean (Fig. 2). At $x = L$ the boundary condition is replaced by $\zeta = \bar{\zeta}(t)$, a prescribed tide elevation considered to be produced by the action of tidal forces on the deep ocean. I assume that

$$\bar{\zeta} = \bar{A} \cos \omega t, \tag{3.1}$$

where $\bar{A}$ and ω are the assigned amplitude and frequency of the tide constituent at the shelf break.

Consider the boundary conditions for the primitive model with difference equations (2.3). In place of (2.5) we now have

$$u_0 = 0; \tag{3.2a}$$

$$\zeta_n = \bar{\zeta} \tag{3.2b}$$

as essential boundary conditions. Hence (2.2a) is applied from $i = 0$ to $n - 1$, and (2.2b) from $i = 1$ to n. At the coast ($i = 0$) the boundary condition is the same as before, so we again get a correct rendition of (2.2a) there by applying rigid-boundary reflection conditions (2.6a) to (2.3a). At the shelf break the auxilliary condition

$$(\partial/\partial t)\, \mu \delta u_n/3 = -c^2 \delta^2 \zeta_n / 2\delta x \tag{3.3}$$

permits us to retain (2.3b), for if (3.3) is subtracted from (2.3b) at $i = n$, the result is equivalent to (2.2b) at $i = n$.

Difference equations (2.3) must be solved now subject to boundary conditions (3.2) and auxiliary end conditions (2.6a) and (3.3). As a preliminary step, we consider the resonances of this model. These can be obtained from the same set of equations by replacing (3.2b) with $\zeta_n = 0$ and (3.3) with free-boundary reflection conditions

$$\zeta_{n+1} = -\zeta_{n-1}; \qquad u_{n+1} = u_{n-1}. \tag{3.4}$$

The solution of this problem is again (2.7a) but with a different array of resonance wave numbers, namely those for which $\cos kL = 0$:

$$k = (\tfrac{1}{2}, \tfrac{3}{2}, \tfrac{5}{2}, \ldots, n - \tfrac{1}{2})\, \pi/L. \tag{3.5}$$

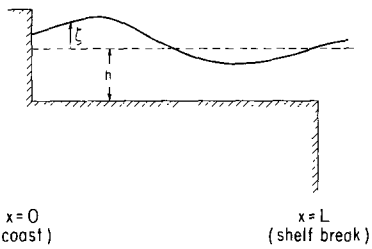

FIG. 2. Definition sketch in x, z-plane.

(The first of these gives the well-known quarter-wave resonance.) The frequency function (2.7b) is unchanged, however, and therefore is still depicted by curve P in Fig. 1, with the attendant aliasing.

Coming to forced oscillations, we know that (2.7) satisfies (2.3) and the homogeneous end conditions (2.6a), (3.2a) at the coast ($x = 0$). Moreover, for each input frequency ω there are two output wave numbers: a low wave number k_1 and its high wave number alias k_2. Our expectation therefore should be that when the additional homogeneous end condition (3.3) and inhomogeneous (3.2b) are imposed, the problem can be solved by a linear combination of two components, each with the form (2.7a):

$$\begin{aligned} \zeta &= (A_1 \cos k_1 x + A_2 \cos k_2 x) \cos \omega t, \\ u/c &= (A_1 \sin k_1 x + A_2 \sin k_2 x) \sin \omega t. \end{aligned} \tag{3.6a}$$

The relation between frequency and wave number is the same as for free oscillations, namely, (2.7b),. but now is more appropriate when inverted:

$$kd = \arccos\left(-2 + \frac{3}{2 \mp (1 - \Omega^2/3)^{1/2}}\right), \tag{3.6b}$$

where $\Omega \equiv \omega d/c$ is the dimensionless input frequency. The upper sign gives the low wave number k_1, the lower sign the alias k_2. The left-hand panel of Fig. 3 is a graph of (3.6b), which in part is identical to curve P of Fig. 1 but is extended to values of

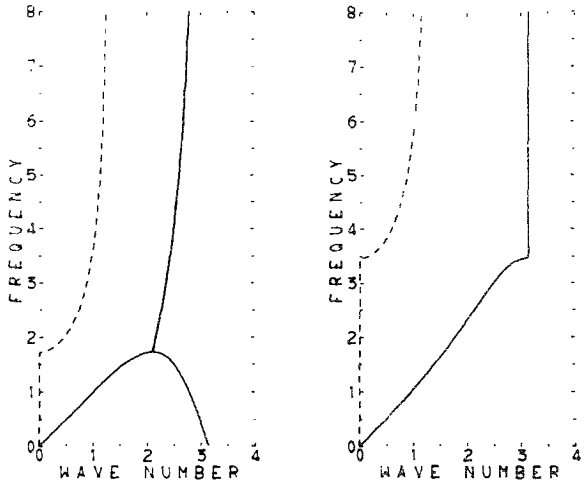

FIG. 3. Response wave number kd as a function of input frequency $\omega d/c$ for forced oscillations of one-dimensional models. Left panel: primitive model, (3.6b); right panel: derivative model, (3.10b). These curves extend those of Fig. 1 to complex wave numbers. Solid lines show real part of kd, dashed lines imaginary part.

$\Omega > 3^{1/2}$ where the output wave numbers are complex. This range has no physical relevance but permits a complete view of the response of the discrete equations.

By requiring the composite solution (3.6a) to satisfy end conditions (3.2b) and (3.3), we get, respectively,

$$C_1 + C_2 = 1; \qquad \tau_1 C_1 + \tau_2 C_2 = 0, \tag{3.7}$$

where $\tau_m \equiv \tan \frac{1}{2} k_m d$ $(m = 1, 2)$ and

$$C_m \equiv (A_m/\bar{A}) \cos k_m L \tag{3.8}$$

is a proxy for the amplitude A_m. It is apparent from (3.8) that each of the component admittances $A_m/\bar{A}$ is a product of the resonance magnification factor sec $k_m L$ and a factor C_m dependent on the resolving power of the grid (as well as on the impressed

TABLE I

Scaled Resonance Frequencies $S \equiv \omega L/\pi c$ vs Scaled Wave Numbers $K \equiv kL/\pi$, with Domain Resolution $L/d = 22$.[a]

	Primitive models			Derivative models		
K	(2.7b)	(4.4b)		(2.13b)	(4.11b)	
0.5	0.50	0.50	1.00	0.50	0.50	41.99
1.5	1.50	1.50	2.95	1.50	1.50	41.75
2.5	2.50	2.50	4.79	2.51	2.51	41.29
3.5	3.50	3.50	6.45	3.54	3.53	40.62
4.5	4.50	4.50	7.87	4.58	4.57	39.78
5.5	5.49	5.49	9.03	5.64	5.62	38.79
6.5	6.47	6.48	9.90	6.74	6.70	37.68
7.5	7.44	7.45	10.50	7.86	7.81	36.50
8.5	8.38	8.40	10.82	9.03	8.95	35.26
9.5	9.28	9.32	10.89	10.23	10.13	34.01
10.5	10.12	10.18	*10.74*	11.49	11.36	32.76
11.5	10.86	10.97	*10.39*	12.78	12.63	31.54
12.5	11.48	11.64	*9.86*	14.13	13.94	30.37
13.5	11.93	12.15	*9.18*	15.51	15.30	29.26
14.5	12.12	12.42	*8.37*	16.92	16.70	28.23
15.5	*12.01*	*12.39*	*7.46*	18.33	18.12	27.30
16.5	*11.49*	*11.96*	*6.45*	19.71	19.50	26.47
17.5	*10.50*	*11.02*	*5.37*	21.02	20.84	25.76
18.5	*8.97*	*9.50*	*4.24*	22.19	22.06	25.18
19.5	*6.91*	*7.38*	*3.06*	23.15	23.08	24.73
20.5	*4.37*	*4.69*	*1.85*	23.85	23.82	24.43
21.5	*1.49*	*1.61*	*0.62*	24.21	24.21	24.28

[a] Alias frequencies are printed in italics. Abnormal frequencies are those in the last and third from the last columns. The continuum resonance frequencies are equal to K.

frequency). I will refer to C_m as the "resonance cross section" of the component. The solution of (3.7) is

$$C_1 = \tau_2/(\tau_2 - \tau_1); \qquad C_2 = \tau_1/(\tau_1 - \tau_2),$$

which, by means of (3.6b), can be converted to

$$C_{1,2} = \tfrac{1}{2}[1 \pm (1 - \Omega^2/3)^{-1/2}] \tag{3.9}$$

(upper sign for C_1, lower for C_2). At high response resolution ($\Omega \ll 1$)—the only situation of physical interest—$C_1 \approx 1 + \Omega^2/12$ and $C_2 \approx -\Omega^2/12$. This shows that if the response is well resolved (that is, $d \ll c/\omega$), the aliased component will not be quantitatively significant except very close to one of the alias resonances.

In both the continuum and discrete models, resonances on the shelf occur at half-integer values of the scaled wave number $K \equiv kL/\pi$. The finite-element model has n of these resonance wave numbers in accordance with (3.5), and as previously noted, the upper one-third are aliased. The corresponding resonance frequencies are fixed by the frequency quation (2.7b) and can be conveniently scaled in a manner analogous to that of k, namely, by $S \equiv \omega L/\pi c = \Omega n/\pi$. (In the continuum, $S = K$.) In Table I the column headed (2.7b) gives values of S for the present model in the particular case $n\,(= L/d) = 22$, a domain resolution used by Gray and Lynch (1979) in one of their examples. Note that the frequency of the slowest alias resonance very nearly coincides with that of the second natural resonance: 1.495 and 1.500, respectively.

The foregoing response characteristics are illustrated in Fig. 4, which shows the

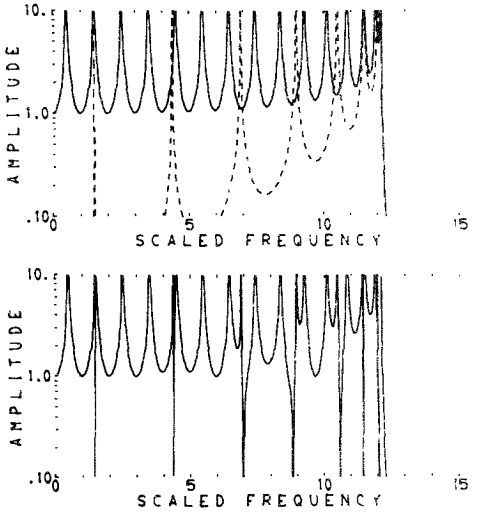

FIG. 4. Response amplitude as a function of scaled input frequency $S \equiv \omega L/\pi c$ in the one-dimensional primitive model. Upper panel: low wave number component $|A_1|$ (solid curve) and high wave number alias $|A_2|$ (dashed curve); lower panel: amplitude $|A_1 + A_2|$ of coastal elevation. The unit of amplitude is the input amplitude $\bar{A}$, and the domain resolution is $L/d = 22$.

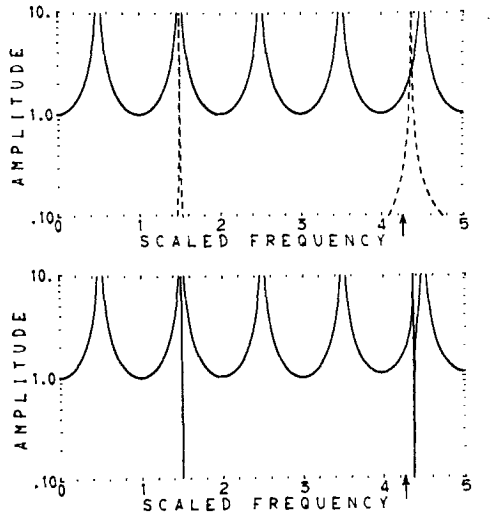

FIG. 5. Same as Fig. 4 but on an expanded frequency scale limited to $0 < S < 5$.

component amplitudes $|A_1|$, $|A_2|$ and the amplitude $|A_1 + A_2|$ of coastal elevation, as a function of S in the case $n = 22$. Figure 5 shows the same curves on an expanded frequency scale in the range $0 < S < 5$. (Larger values of S are not of practical interest because the wave lengths they excite are too small to be well resolved.) The pathologically small cross section of the first alias resonance is apparent from Fig. 5, and is more clearly displayed on the greatly expanded frequency scale of Fig. 6. The second alias is somewhat more prominent (Fig. 5). An interesting feature of Fig. 4 is

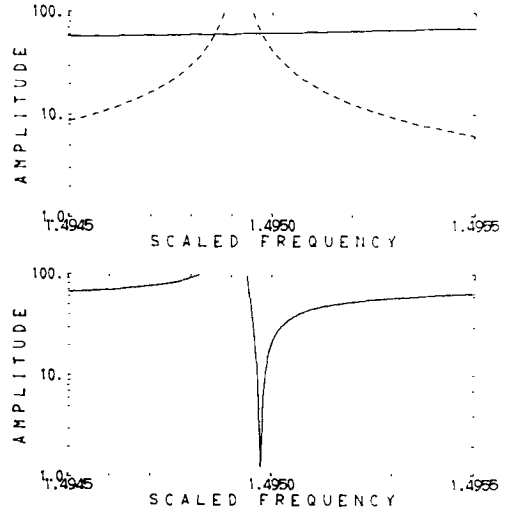

FIG. 6. Detail of Fig. 5 showing the first alias resonance on a greatly expanded frequency scale.

the abrupt attenuation of the response when the input frequency exceeds the critical value $c\,3^{1/2}/d$, beyond which there are no resonances. This corresponds to a scaled frequency $S = n\,3^{1/2}/\pi$ ($= 12.13$ for $n = 22$). If the discrete model is forced at a frequency greater than this, it does not permit waves to propagate, thus causing the excitation to be trapped at the source. (The remedy is of course simply to choose a much smaller value of d!)

In their first example Gray and Lynch (1979) considered a channel of depth $h = 30$ ft (9.14 m), length $L = 22d$ with $d = 1.3 \times 10^5$ ft (39.6 km), and input period 12.0 hr. These data (and $g = 9.8\ \text{ms}^{-2}$) give a scaled frequency $S = 4.26$ (indicated by the arrow in Fig. 5), which fortuitously is close to the second alias resonance and should therefore be expected to produce a noisy response. This expectation is confirmed by exhibiting the response as a function of x at frequency $S = 4.26$ (Fig. 7). If the input frequency is shifted to that of the M_2 tide (period 12.42 hr), the scaled frequency is reduced by about 3.4% to $S = 4.12$. This slight shift away from the alias resonance gives a smoother response with noise amplitude only about half that shown in Fig. 7, a result consistent with Fig. 5.

We turn next to a brief examination of the response of the finite-element equations (2.9) based on Stokes/Helmholtz potentials. The problem to be solved is defined by the difference equations (2.11) from $i = 0$ to $n - 1$, the rigid-boundary reflection condition (2.12a) needed to make (2.11) equivalent to (2.10) at the coast, and the boundary condition $\zeta_n = \bar{\zeta}$ at the shelf break, with $\bar{\zeta}$ is in (3.1). For free oscillations the solution is formally identical to (2.13), but with half-integer values of the scaled wave number $K \equiv kL/\pi$, as in (3.5). It can further be adapted to forced oscillations merely by replacing σ in (2.13a) with ω:

$$\begin{aligned} \zeta &= A \cos kx \cos \omega t, \\ \phi\omega/g &= A \cos kx \sin \omega t, \end{aligned} \tag{3.10a}$$

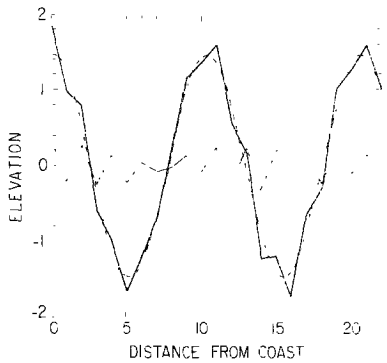

FIG. 7. Surface elevation versus x/d for a scaled input frquency $S = 4.26$, in the one-dimensional primitive model. The dashed curve is the continuum response, the approximating solid curve is the discrete response, and the smaller-amplitude solid curve is the piece-wise-linear truncation error formed from discrete minus continuum nodal values. The unit of elevation is the input amplitude $\bar{A}$.

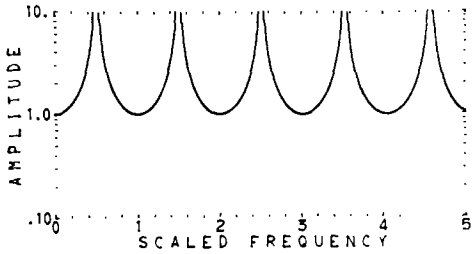

FIG. 8. Amplitude $|A|$ of coastal elevation as a function of scaled input frequency $\omega L/\pi c$, in the one-dimensional derivative model.

and inverting the frequency equation (2.13b):

$$kd = \arccos[-2 + 3/(1 + \Omega^2/6)], \tag{3.10b}$$

where $\Omega \equiv \omega d/c$ as before. The right-hand panel of Fig. 3 is a graph of (3.10b), and the column headed (2.13b) in Table I gives the resonance frequencies for this model. (The trapping frequency is exactly twice that of the preceding model.)

The above solution has only one component because there is no aliasing in the derivative model. It is completed by the use of the boundary condition $\zeta_n = \bar{\zeta}$ to fix the output amplitude:

$$A = \bar{A} \sec kL. \tag{3.11}$$

Figure 8 shows $|A|$ as a function of scaled frequency. Since $|A|$ is equal to the coastal amplitude of ζ, Fig. 8 is comparable to both panels of Fig. 5. Absence of aliasing evidently provides a smoother response, as shown in Fig. 9. Although the *rms* error is about the same as in Fig. 7, the scale of the error is now that of the response, instead of being primarily "$2\delta x$ noise."

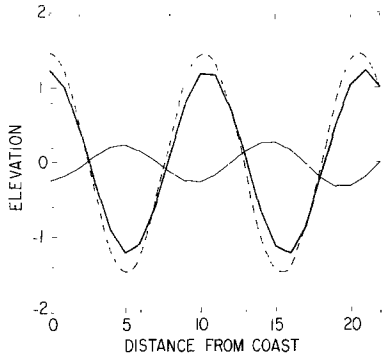

FIG. 9. Surface elevation versus x/d for $S = 4.26$, in the one-dimensional derivative model. The curves are analogous to those of Fig. 7.

The foregoing analysis shows how small-scale error can arise from aliasing in a one-dimensional model of tidal type, and how such errors can be avoided. An extension of the analysis to two dimensions can be made with only moderate complications, and is carried out in the next section.

4. Two-Dimensional Models

The extension of finite-element equations (2.2) to a two-dimensional domain is

$$\int \alpha^i(\partial\zeta/\partial t)\,dS = \int \nabla\alpha^i \cdot \boldsymbol{lu}\,dS, \tag{4.1a}$$

$$\int \beta^i(h^{-1}\,\partial\boldsymbol{lu}/\partial t)\,dS = \int \beta^i(-g\nabla\zeta)\,dS, \tag{4.1b}$$

where dS is an element of area. I will limit this account to purely longitudinal oscillations in which the volume transport $\boldsymbol{lu}$ has zero y-component, so there are again only two dependent variables ζ and u, each a function only of x. The basis functions, however, are two-dimensional, α being the pyramidal analogue of a two-dimensional delta function and β either like α (primitive model) or proportional to the gradient of α (derivative model).

The domain of concern to us is the infinite strip in the x, y-plane between the coast $x=0$ and the shelf break $x=L$. The left panel of Fig. 10 illustrates a "homogeneous" triangulation of this domain in which the elements are identical in size and shape and all internal nodes have the same number of neighbor links. In this grid the element triangles are isosceles with altitude d, and the number of links is six.

It is a simple matter to show that when the motion is purely longitudinal and the basis functions piecewise linear, the difference equations obtained from (4.1) with homogeneous triangulation are identical to those derived from one-dimensional models in the preceding sections. (This is not surprising in view of the arrangement of links along equally-spaced lines parallel to the y-axis.) All of the results obtained to this point therefore apply to the left panel of Fig. 10.

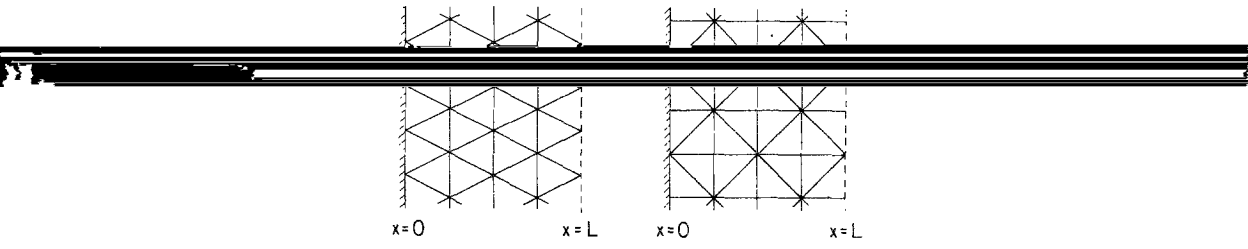

Fig. 10. Two triangulations for discussion of effects of two-dimensionality.

The situation is different, however, for the right panel of Fig. 10. This well-known "inhomogeneous" triangulation also consists of identical isosceles triangles but the links parallel to the x-axis create two distinct lattices, in one of which each node is linked to four neighbors and in the other to eight. (If the links parallel to the x-axis were omitted, the triangulation would be homogeneous.) In these circumstances we must provide for the possibility that ζ, u on one lattice may differ from ζ, u on the other for the same value of x.

Let ζ, u denote values on the lattice with four links and ζ', u' on the one with eight. Then the difference equations that arise from (4.1) for a primitive model with piecewise-linear bases are

$$(\partial/\partial t)(\zeta + \mu^2\zeta')/2 = -\mu\delta u'/\delta x, \tag{4.2a}$$

$$(\partial/\partial t)(u + \mu^2 u')/2 = -c^2\mu\delta\zeta'/\delta x, \tag{4.2b}$$

at an interior ζ, u node and

$$(\partial/\partial t)(\zeta' + 2\mu^2\zeta' + \mu^2\zeta)/4 = -\mu\delta(u' + u)/2\delta x, \tag{4.3a}$$

$$(\partial/\partial t)(u' + 2\mu^2 u' + \mu^2 u)/4 = -c^2\mu\delta(\zeta' + \zeta)/2\delta x, \tag{4.3b}$$

at an interior ζ', u' node. The operators μ and δ are those defined in (2.4).

At the coast we have as before $u = 0$ and $u' = 0$ as essential conditions in place of (4.2b) and (4.3b), while (4.2a) and (4.3a) can be retained as the correct rendition of (4.1a) provided we adopt rigid-boundary reflection conditions (2.6a) for both ζ, u and ζ', u'. At the shelf break where ζ and ζ' are subject to essential conditions, we do not apply (4.1a) and hence neither (4.2a) nor (4.3a). In the case of free oscillations these essential conditions are $\zeta = 0$ and $\zeta' = 0$. Moreover, at the shelf break (4.2b) and (4.3b) can be retained as the correct rendition of (4.1b) provided the free-boundary reflection conditions (3.4) are adopted for both ζ, u and ζ', u'. In that case the solution of (4.2), (4.3) for free oscillation is

$$\begin{aligned} (\zeta, \zeta') &= (1, \lambda) A \cos kx \cos \sigma t, \\ (u, u')/c &= \pm(1, \lambda) A \sin kx \sin \sigma t, \\ \lambda &\equiv -2/[1 \mp (7 + 2\cos kd)^{1/2}], \end{aligned} \tag{4.4a}$$

$$\sigma d/c = (4 \sin kd)/[(7 + 2\cos kd)^{1/2} \pm \cos kd]. \tag{4.4b}$$

As before, the resonance wave numbers are those that make $\cos kL = 0$, namely, (3.5). It is apparent from (4.4a) that (ζ, u) is not necessarily equal to (ζ', u') for the same x, t. The deviation between the two lattices is controlled by the dispersion parameter λ.

Frequency equation (4.4b) provides an interesting comparison with its one-dimensional analogue (2.7b). As shown by the P-curves in Fig. 11 there are now two branches instead of one, corresponding to the sign alternative in (4.4b). They are identified in the figure as PN ("normal" P, obtained by taking the upper sign in

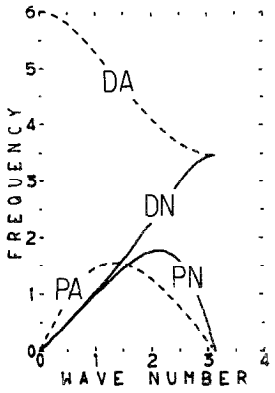

FIG. 11. Resonance frequency $\sigma d/c$ as a function of wave number kd for free longitudinal oscillations in a domain triangulated as in the right panel of Fig. 10. Curves P (primitive model) are from (4.4b), curves D (derivative model) from (4.11b), and in each case N (normal) and A (abnormal) signify respectively the upper and lower sign alternatives in these equations. The two N branches very nearly coincide with the P and D curves of Fig. 1.

(4.4b)) and *PA* ("abnormal" *P*, from the lower sign). Both branches are folded back to zero frequency at $kd = \pi$, so we now have a double aliasing effect. The *PN* branch has the reassuring property that it differs from curve *P* of Fig. 1 only slightly (at most 2.5% in frequency over the unaliased range of wave numbers), despite the fact that the algebraic relations (2.7b) and (4.4b) are manifestly different. The abnormal branch *PA* arises from the inhomogeneity of the grid triangulation (Fig. 10, right panel), which as previously noted forms two interlacing lattices of nodes.

The nature of the abnormal solution can be examined by considering the limit of (4.4) at high resolution $kd \to 0$. Then for the upper (normal) sign, $\lambda \to 1$ so $(\zeta', u') \to (\zeta, u)$ and (4.4) converges to the continuum solution with $\sigma \to kc$. The lower sign, however, makes $\lambda \to -\frac{1}{2}$ so $(\zeta', u') \to -\frac{1}{2}(\zeta, u)$. In this case nodal values on the two lattices fail to coalesce and (4.4) converges to

$$(\zeta, \zeta') = (1, -\tfrac{1}{2})\, A \cos kx \cos \sigma t,$$
$$(u, u')/c = (-1, \tfrac{1}{2})\, A \sin kx \sin \sigma t,$$
$$\sigma = 2kc,$$

clearly not a physically appropriate solution. The existence of this abnormal solution arises from the structure of the governing difference equations (4.2), (4.3). In the limit associated with the lower sign in (4.4), the difference equations converge to abnormal continuum equations

$$\partial\zeta/\partial t = 2\partial u/\partial x; \qquad \partial u/\partial t = 2gh\, \partial\zeta/\partial x.$$

The upper sign, on the other hand, which leads to coalescence of nodal values on the two lattices, causes (4.2), (4.3) to converge to the proper continuum equations (2.1).

Turning to forced oscillations, we can follow a procedure entirely analogous to that used in the one-dimensional case. At the shelf break the boundary condition is

$$(\zeta, \zeta') = (1, 1)\,\bar{A} \cos \omega t. \tag{4.5}$$

Further, (4.2b) and (4.3b) will correctly render (4.1b) at $i = n$ if supplemented, respectively, by

$$(\partial/\partial t)\,\mu\delta u'_n/4 = -c^2\delta^2\zeta'_n/2\delta x, \tag{4.6a}$$

$$(\partial/\partial t)\,\mu\delta(2u'_n + u_n)/4 = -c^2\delta^2(\zeta'_n + \zeta_n)/4\delta x. \tag{4.6b}$$

Now, we know that (4.4) satisfies all conditions of the problem except the two inhomogeneous end conditions (4.5) and the two homogeneous (4.6). Since there are four output wave numbers for each input frequency, we should expect a response consisting of a superposition of four components, each with the form (4.4a):

$$\begin{aligned}(\zeta, \zeta') &= \sum_{m=1}^{4} (1, \lambda_m) A_m \cos k_m x \cos \omega t, \\ (u, u')/c &= \sum_{m=1}^{4} (1, \lambda_m)(\pm A_m) \sin k_m x \sin \omega t.\end{aligned} \tag{4.7a}$$

The sign alternative here is the same as that in (4.4). I will adopt the convention that components $m = 1, 2$ correspond to the upper sign (the normal components) and $m = 3, 4$ to the lower sign (abnormal components). Each of these pairs has a low wave number, respectively, k_1 and k_3, and a high wave number alias, k_2 and k_4. (We can also properly regard k_3 and k_4 as well as k_2 as aliases of k_1.) The frequency equation (4.4b) cannot be solved explicitly for kd but it can be rewritten as a quartic equation for $\cos kd$:

$$\begin{aligned}0 = {} & (16 + \Omega^2)^2 (\cos kd)^4 + 4\Omega^2(16 - \Omega^2)(\cos kd)^3 \\ & - (16 - \Omega^2)(16 - 5\Omega^2)(\cos kd)^2 \\ & - 4\Omega^2(16 - 7\Omega^2)(\cos kd) + (16 + 7\Omega^2)^2,\end{aligned} \tag{4.7b}$$

where $\Omega \equiv \omega d/c$. The left panel of Fig. 12 shows the result of solving (4.7b) for a range of values of Ω that extends to the region of complex wave numbers. It is analogous to the left panel of Fig. 3 (the one-dimensional model). The columns headed (4.4b) in Table I list the two sets of resonance frequencies in this model.

It remains to find the four amplitude factors A_m in (4.7a), and for this purpose we have only to invoke the four end conditions at $x = L$. The following four

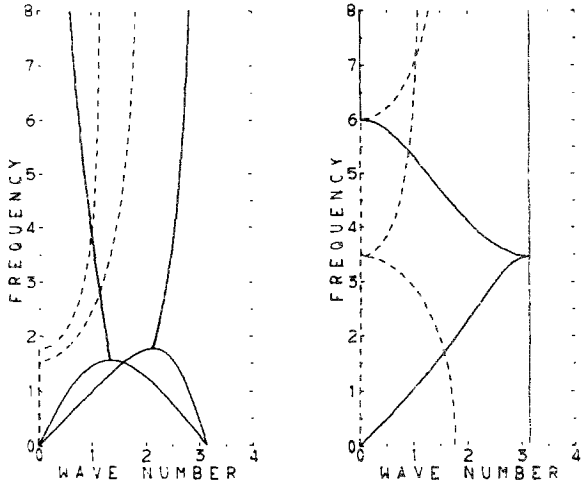

FIG. 12. Response wave number kd as a function of input fresuency $\omega d/c$ for forced oscillations of two-dimensional models. Left panel: primitive model, (4.7b); right panel: derivative model, (4.12b). Solid lines show real part of kd, dashed lines imaginary part. Compare this diagram with its one-dimensional analogue, Fig. 3.

simultaneous equations emerge from substitution of (4.7a) respectively into (4.5) and (4.6):

$$\sum_{m=1}^{4} (1, \lambda_m) C_m = (1, 1), \tag{4.8a}$$

$$\sum_{m=1}^{4} (1, \lambda_m) \tau_m C_m = (0, 0), \tag{4.8b}$$

where C_m is the resonance cross section defined in (3.8) and $\tau_m \equiv \pm \tan \frac{1}{2} k_m d$ (upper sign for $m = 1, 2$; lower sign for $m = 3, 4$). Equations (4.8) are clearly the analogues of (3.7).

Since λ_m and τ_m in (4.8) are known functions of $k_m d$, the four resonance cross sections C_m can be calculated from (4.8) as functions of input frequency, and the corresponding amplitudes can then be evaluated from (3.8). The two upper panels of Fig. 13 display $|A_1|$, $|A_2|$ and $|A_3|$, $|A_4|$, respectively, for the same domain resolution as used previously ($n = 22$). The top panel is very nearly identical to the upper panel of Fig. 5, its one-dimensional analogue.

As in one dimension the amplitude of normal component A_1 is dominant when the response is well resolved ($\Omega \ll 1$), unless one of the other components is close to resonance. In the range $0 < S < 2$, for example, there are six resonances as follows (see Table I):

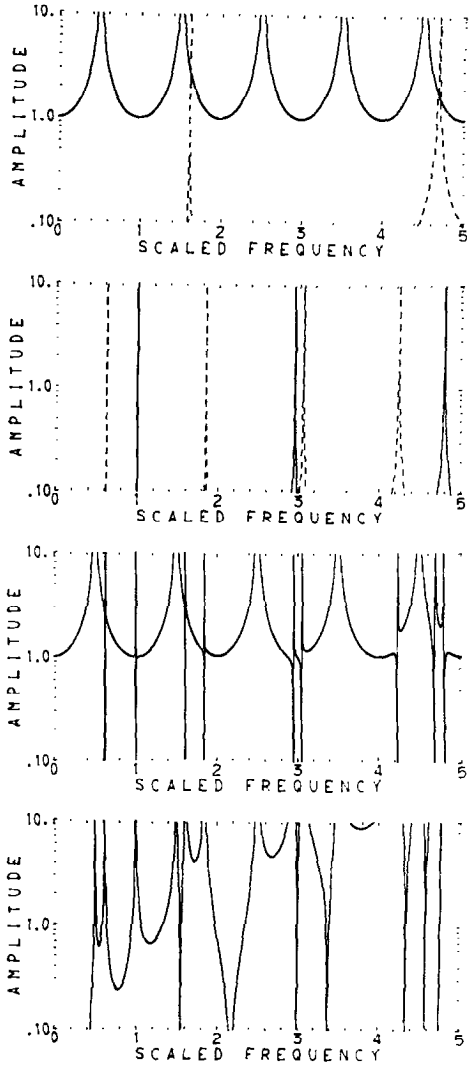

FIG. 13. Response amplitude as a function of scaled input frequency $\omega L/\pi c$ in the two-dimensional primitive model. From top to bottom the four panels are: normal amplitude $|A_1|$ (solid curve) with its alias $|A_2|$ (dashed curve); second, abnormal amplitude $|A_3|$ (solid curve) with its alias $|A_4|$ (dashed curve); third, amplitude $|A_1+A_2+A_3+A_4|$ of coastal elevation ζ; fourth, the dispersion $100\,|\zeta-\zeta'|$. Compare the first and third panels with their one-dimensional analogous in Fig. 5.

S	Type of resonance
0.50	first normal
0.62	first abnormal alias
1.00	first abnormal
1.50	second normal
1.61	first normal alias
1.85	second abnormal alias

In one dimension the abnormal resonances are absent and the first alias resonance coincides (at high resolution) with the second normal resonance 1.50. Thus, in this important range of input frequency the possibility of generating $2\delta x$ noise is virtually nil in a one-dimensional model. In two dimensions the situation is quite different, because in addition to the normal resonances at 0.5 and 1.5 there are (in the range $0 < S < 2$) four anomalous resonances, any one of which can produce $2\delta x$ noise. Despite this fact, the possibility that such noise will be excited at high resolution ($\Omega \ll 1$) is extremely limited because the cross section of each of the anomalous resonances is of order Ω^2. In other words, extraordinarily precise tuning would be neded to excite these components. However, if the response resolution is poor, $2\delta x$ noise will be almost unavoidable.

According to (4.7a) the amplitudes of ζ and ζ' at the coast $x = 0$ are, respectively,

$$|\zeta| = \left| \sum_{m=1}^{4} A_m \right|; \qquad |\zeta'| = \left| \sum_{m=1}^{4} \lambda_m A_m \right|.$$

The first of these is shown as a function of scaled frequency in the third panel of Fig. 13. Since in the range $0 < S < 5$ there is very little difference between ζ and ζ' except near resonances, I have plotted the dispersion $100\,|\zeta - \zeta'|$ (bottom panel of Fig. 13) rather than $|\zeta'|$ as the companion to $|\zeta|$. Figure 14 displays ζ and its "ghost" ζ' as functions of x/d for the same scaled input frequency $S = 4.26$ as used in Fig. 7 (the one-dimensional analogue of Fig. 14). The noise level in this response is much higher than in one dimension because of the close proximity of the aliased abnormal resonance at $S = 4.24$ (see Table I). In one dimension the resonance closest to $S = 4.26$ is at 4.37.

Finally, we must compare the preceding model with the finite-element model obtained by using Stokes/Helmholtz potentials in two dimensions:

$$\int \alpha^i(\partial\zeta/\partial t)\, dS = \int \nabla\alpha^i \cdot (-h\nabla\phi)\, dS, \tag{4.9a}$$

$$\int \nabla\alpha^i \cdot (\partial h\nabla\phi/\partial t)\, dS = \int \nabla\alpha^i \cdot (gh\nabla\zeta)\, dS. \tag{4.9b}$$

As in one dimension, (4.9b) requires $\partial\phi/\partial t = g\zeta$ (apart from an irrelevant additive function of t alone), so ϕ can be eliminated from (4.9a) by applying $\partial/\partial t$. This gives

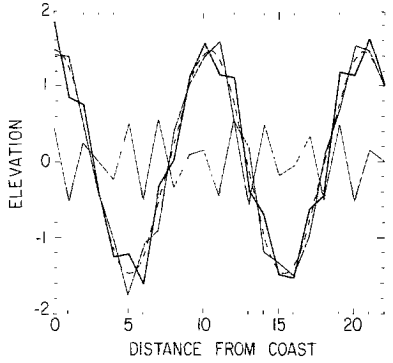

FIG. 14. Surface elevations ζ (heavy solid curve), ζ' (light solid curve), and the continuum solution (dashed curve) vs x/d for a scaled input frequency $S = 4.26$ in the two-dimensional primitive model. This diagram is the two-dimensional analogue of Fig. 7, except that here the small-amplitude curve is $\zeta - \zeta'$.

the finite-element wave equation. Let ζ, ϕ and ζ', ϕ' denote nodal values on the two lattices of Fig. 10 (right panel) and consider only longitudinal oscillations, so that each of the dependent variables is a function only of x. Then for piecewise-linear bases and uniform depth, the finite-element wave equation leads to the following difference equations, respectively at interior ζ and ζ' nodes:

$$(\partial^2/\partial t^2)(\zeta + \mu^2\zeta')/3 = c^2[\delta^2\zeta' + 4(\zeta' - \zeta)]/(\delta x)^2, \tag{4.10a}$$

$$(\partial^2/\partial t^2)(\zeta' + 2\mu^2\zeta' + \mu^2\zeta)/3 = c^2[\delta^2\zeta + 4(\zeta - \zeta')]/(\delta x)^2. \tag{4.10b}$$

At $x = 0$ we obtain a correct rendition of (4.9a) by using rigid-boundary reflection conditions $\zeta_{-1} = \zeta_1$ and $\zeta'_{-1} = \zeta'_1$ in (4.10a). At the shelf break $x = L$, (4.9b) and (4.10b) are replaced by the boundary condition (4.5). The solution of this problem is, for free oscillations ($\bar{A} = 0$ in (4.5))

$$(\zeta, \zeta') = (1, \lambda) A \cos kx \cos \omega t,$$

$$(\phi, \phi')\, \sigma/g = (1, \lambda) A \cos kx \sin \omega t, \tag{4.11a}$$

$$\lambda \equiv -2/[1 \mp (7 + 2\cos kd)^{1/2}],$$

$$\frac{\sigma d}{c} = 12^{1/2} \left(1 - \frac{2(1 + \cos kd)}{\cos kd \pm (7 + 2\cos kd)^{1/2}}\right)^{1/2}. \tag{4.11b}$$

The resonance wave numbers are again the ones that make $\cos kL = 0$, namely, (3.5).

Frequency equation (4.11b) is plotted as the D-curves in Fig. 11. As in the preceding model, for each wave number there are two resonance frequencies and thus two free modes. One (labeled DN, from taking the upper sign in (4.11b)) is normal in the sense that it approximates the continuum response. (It differs from curve D in Fig. 1—the one-dimensional analogue—by at most 1.4% in frequency.) The

abnormal branch (DA) arises from the inhomogeneity of the grid triangulation (Fig. 10, right panel).

To solve (4.10) subject to the inhomogeneous conditions (4.5), we need a linear combination of two components. At first sight it seems that only one component is available because the D-curves in Fig. 11 show the wave number as a single-valued function of frequency. However, these curves depict only the aspect of (4.11b) that corresponds to free oscillations, and therefore to real wave numbers k. In fact, as will be seen below, (4.11b) does indeed make the wave number a double-valued function of frequency if complex wave numbers are taken into account. The forced response therefore is expressible as a linear combination of two components:

$$\begin{aligned}(\zeta, \zeta') &= \sum_{m=1}^{2} (1, \lambda_m) A_m \cos k_m x \cos \omega t, \\ (\phi, \phi')\, \omega/g &= \sum_{m=1}^{2} (1, \lambda_m) A_m \cos k_m x \sin \omega t.\end{aligned} \tag{4.12a}$$

Here k_1 and k_2 are wave numbers derived from inversion of (4.11b):

$$kd = \arccos\left(-1 + \frac{2(1-\theta)}{\theta \pm (1 + 2\theta + 2\theta^2)^{1/2}}\right), \tag{4.12b}$$

where $\theta \equiv \Omega^2/12$ (with $\Omega \equiv \omega d/c$).

The right-hand panel of Fig. 12 maps the two functions (4.12b). The upper sign gives the normal branch of kd, the lower sign the abnormal branch. The normal wave number k_1 is real in the range $0 \leqslant \Omega \leqslant 3$ and omplex for $\Omega > 3$. The abnormal k_2 is real in $3 \leqslant \Omega \leqslant 6$ and complex for $0 \leqslant \Omega < 3$ and $\Omega > 6$. In particular, in the range $0 < \Omega \ll 1$ of physical interest (4.12b) gives

$$\begin{aligned}k_1 d &= \Omega + O(\Omega^3), \\ k_2 d &= \pi + i[\operatorname{arc\,cosh} 3 + O(\Omega^2)].\end{aligned}$$

The abnormal component is evidently strongly trapped at the source, its attenuation being at the rate of approximately $\exp(-\operatorname{arc\,cosh} 3) = 3 - 8^{1/2} = 0.17$ per grid interval.

Formal completion of the solution comes from imposing boundary condition (4.5) on (4.12a) at $x = L$:

$$\sum_{m=1}^{2} (1, \lambda_m) C_m = (1, 1), \tag{4.13}$$

where C_m is the resonance cross section defined in (3.8). The solution of (4.13) is

$$C_1 = \frac{\lambda_2 - 1}{\lambda_2 - \lambda_1}; \qquad C_2 = \frac{\lambda_1 - 1}{\lambda_1 - \lambda_2},$$

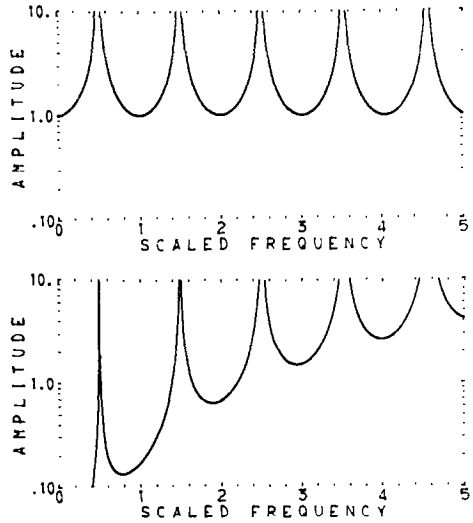

FIG. 15. Amplitude $|\zeta| \approx |A_1|$ of coastal elevation (upper panel) and the dispersion $100\,|\zeta - \zeta'|$ (lower panel) in the two-dimensional derivative model. (The abnormal amplitude A_2 is negligible.) Compare the upper panel with its one-dimensional analogue, Fig. 8.

which, by means of (4.12b) can be converted to

$$C_{1,2} = \tfrac{1}{2}[1 \pm (1 + 2\theta + 2\theta^2)^{-1/2}]. \tag{4.14}$$

At high response resolution ($\Omega \ll 1$) the cross sections are $C_1 \approx 1 - \Omega^2/24$ and $C_2 \approx \Omega^2/24$, thus assuring that the abnormal part of the response is small.

Figure 15 shows normal amplitude $|A_1|$ calculated from the cross section (4.14) as

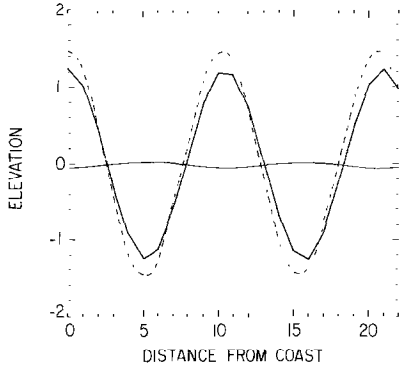

FIG. 16. Surface elevations ζ (solid curve) and the continuum solution (dashed curve) versus x/d for a scaled input frequency $S = 4.26$ in the two-dimensional derivative model. The small-amplitude curve is $\zeta - \zeta'$. Compare this diagram with its one-dimensional analogue, Fig. 9 (where, however, the small-amplitude curve is ζ minus the continuum solution).